Published in final edited form as:
Nucl Med Biol. 2014 March ; 41(3): 248–253. doi:10.1016/j.nucmedbio.2013.12.010.

Al^{18}F-NODA-butyric acid: biological evaluation of a new PET renal radiotracer

Malgorzata Lipowska[a,*], **Jeffrey Klenc**, **Dinesh Shetty**[a], **Jonathon A. Nye**[a], **Hyunsuk Shim**[a,b], and **Andrew T. Taylor**[a]

[a]Department of Radiology and Imaging Sciences, Emory University, Atlanta, GA 30322, USA

[b]Winship Cancer Institute, Emory University, Atlanta, GA 30322, USA

Abstract

Introduction—Renal scintigraphy is an important imaging modality for the diagnosis and management of a variety of renal diseases including obstruction and renovascular hypertension as well as the evaluation of absolute and relative kidney function. The goal of this work was to evaluate Al^{18}F-NODA-butyric acid (Al^{18}F-**1**) as a potential PET tracer to image the kidneys and monitor renal function by comparing its pharmacokinetic properties with those of ^{131}I-*o*-iodohippurate (^{131}I-OIH), the radioactive standard for the measurement of effective renal plasma flow.

Methods—Al^{18}F-**1** was prepared in aqueous conditions using a one-pot Al^{18}F-radiofluorination method and its radiochemical purity was determined by HPLC. Biodistribution studies, using ^{131}I-OIH as an internal control, were performed in normal rats and in rats with renal pedicle ligation. *In vitro* stability and metabolism of Al^{18}F-**1** were analyzed by HPLC. Dynamic microPET/CT studies were conducted in normal rats.

Results—Al^{18}F-**1** showed excellent stability in vitro and in vivo. Biodistribution studies in normal rats and in rats with simulated renal failure confirmed that Al^{18}F-**1** was exclusively cleared through the renal-urinary pathway and that the hepatic/gastrointestinal activity was less for Al^{18}F-**1** than for ^{131}I-OIH both at 10 and 60 min. Dynamic PET showed a rapid transit of Al^{18}F-**1** through the kidneys into the bladder.

Conclusion—These results suggest that the easily labeled Al^{18}F-based compounds provide a highly promising approach for the development of a PET renal radiotracer that combines superior imaging qualities with a reliable measure of effective renal plasma flow.

Keywords

Al^{18}F-NODA-butyric acid; Aluminum fluoride; Renal radiopharmaceutical; Kidney; PET ^{18}F

[*]Corresponding Author: Department of Radiology and Imaging Sciences, Emory University, 1364 Clifton Road, NE, Atlanta, GA 30322, USA; telephone: (404)-727-3510, fax: (404)-727-3488, mlipows@emory.edu.

1. Introduction

Chronic kidney disease (CKD) is recognized as worldwide public health problem [1, 2]. Renal scintigraphy can help address this problem by providing a non-invasive method of evaluating a variety of known or suspected renal diseases and of monitoring renal function. Radionuclide renography also has the advantage of using a subpharmacological dose of radiotracer thus avoiding allergic reactions or toxic effects. Currently, renal scintigraphy is performed using dynamic planar gamma imaging. The best radiotracers are those labeled with technetium-99m (^{99m}Tc) since this radionuclide has almost ideal nuclear properties ($t_{1/2}$ = 6 h, γ-radiation of 140 keV, no beta radiation), can be practically eluted from a ^{99}Mo/^{99m}Tc generator, and kits for the routine preparation of ^{99m}Tc radiotracers are readily available. The most utilized ^{99m}Tc renal radiotracers (Fig. 1) are (1) ^{99m}Tc-diethylenetriamine-pentaacetic acid (^{99m}Tc-DTPA) which is cleared exclusively by glomerular filtration and can be used to measure glomerular filtration rate (GFR) [3, 4]; (2) ^{99m}Tc-mercaptoacetyltriglycine (^{99m}Tc-MAG3) which is excreted primarily by tubular secretion and has become the radiopharmaceutical of choice for evaluation of effective renal plasma flow (ERPF) [5–7]; and (3) ^{99m}Tc-dimercaptosuccinic acid (^{99m}Tc-DMSA) which is retained in the renal tubules and is used clinically for morphological evaluation of the kidneys [8, 9]. Recently, we have identified a new ^{99m}Tc renal tracer, ^{99m}Tc(CO)$_3$-nitrilotriacetic acid (^{99m}Tc-NTA), which has showed pharmacokinetic properties almost identical to those of ^{131}I-*o*-iodohippurate (^{131}I-OIH) in rats, healthy volunteers and in patients with chronic kidney disease [10–12]. We compared ^{99m}Tc-NTA to ^{131}I-OIH since ^{131}I-OIH is still regarded as the radioactive standard for the non-invasive measurement of ERPF [13] even though it is no longer clinically available due to the beta emission of ^{131}I resulting in relative high radiation dose to kidney and thyroid in patients with impaired renal function [14].

The recent lack of availability of ^{99m}Tc due to a shortage of ^{99}Mo supply [15], coupled with favorable physical properties of fluorine-18 (^{18}F) radionuclide ($t_{1/2}$ = 109.8 min, β^+, 97%) and the sensitivity and spatial resolution of positron emission tomography (PET) have stimulated efforts to develop PET renal radiotracers [16–20]. Schnöckel et al. first validated an ^{18}F-PET-based method to quantify renal function in rats using ^{18}F-fluoride and found that PET approach could provide a reproducible and non-invasive estimation of renal function in small animals [18]; this study provided proof of concept but ^{18}F-fluoride could not function as a dedicated renal radiopharmaceutical because of localization in the bone [21, 22]. Two other ^{18}F-labeled agents were recently assessed in rats as potential PET renal radiopharmaceuticals [19, 20]. One of them, ^{18}F-*p*-fluorohippurate (^{18}F-PFH) was found to be rapidly and exclusively cleared by the kidneys [19] and the quality of its renogram and images obtained by dynamic PET studies were reported to be better than those obtained with ^{99m}Tc-MAG3 dynamic planar imaging studies [23]. However, the ^{18}F-PFH synthesis was long and required a four-step, two-pot procedure using a prosthetic group, ^{18}F-*N*-succinimidyl-4-fluorobenzoate (^{18}F-SFB). The synthesis of the second tracer, ^{18}F-*m*-cyano-*p*-fluorohippurate (^{18}F-CNPFH), utilized the simpler process of direct onestep nucleophilic aromatic substitution reaction but biodistribution and dynamic PET imaging studies in rats showed that ^{18}F-CNPFH would not be an effective renal imaging agent because it was eliminated by both renal and hepatobiliary pathways [20].

The development of functional PET imaging of the kidney has been slow due to the widespread availability of single photon planar renal imaging coupled with the lack of rapid and easily accessible ^{18}F labeling procedures. Introduction of ^{18}F-fluorine into a biomolecule usually requires formation of F-C bond; typically a challenging procedure due to multiple steps and harsh reaction conditions [24]. Recently, a new radiofluorination method using aluminum fluoride (Al^{18}F) complex formation was reported in an attempt to

address the difficulty in ^{18}F labeling of biomolecules [25–28]. This aqueous ^{18}F radiolabeling method via $Al^{18}F$ chelation is not only simple, straightforward and fast (typically 30–40 min), but it resembles the radiometal labeling process thus, it can be easily adopted to kit formulation [29]. The latest first-in-man study of $Al^{18}F$-NOTA-PRGD2 (obtained from a lyophilized kit) in patients with lung cancer showed excellent *in vivo* stability of $Al^{18}F$-based radiotracer and its suitability for PET imaging [30]. Here we describe the evaluation of a new $Al^{18}F$-NODA-butyric acid complex as a potential renal PET tracer by comparing its pharmacokinetic properties to those of ^{131}I-OIH in normal rats and in rats with renal failure.

2. Materials and Methods

2.1. General

1,4,7-triazacyclononane (TACN) was purchased from CheMatech (Dijon, France) and *tert*-butyl bromobutyrate was purchased from AstaTech Inc (Bristol, US). All other chemicals were purchased from Sigma/Aldrich (St. Louis, US). 2,2′-(7-(3-carboxypropyl)-1,4,7-triazacyclononane-1,4-diyl)diacetic acid (NODA-butyric acid, **1**) was prepared as previously reported [31]. [^{18}F]fluoride in water (swfi) was obtained from Emory CSI Radiopharmacy for biodistrubution studies and was purchased from PETNET Solutions at Emory University Yerkes National Primate Center for microPET imaging studies. Trap/release cartridges model DW-TRC were obtained from D&W, Inc. (Oakdale, TN). ^{131}I-OIH was prepared as previously described [10]. ^1H NMR spectra were recorded on INOVA-400 (400 MHz) spectrometer. The spectra were obtained at room temperature in $CDCl_3$ or D_2O and were referenced to the residual solvent peak. Chemical shifts (δ) were reported in ppm downfield from tetramethylsilane. HRMS were measured by the Emory University Mass Spectrometry Center and were recorded on a Thermo-Finnegan LTQ FTMS spectrometer. The synthesized compounds were characterized by ^1H NMR, MS and HPLC and their purity was > 95%. The HPLC chromatograms for the ^{18}F tracer were obtained by use of a Beckman System Gold Nouveau apparatus equipped with a model 170 radiometric detector and a model 166 ultraviolet light-visible light detector, and a Beckman C18 RP Ultrasphere octyldecyl silane column (5-μm, 4.6 × 250 mm). The flow rate of the mobile phase was 1 mL/min, the mobile phase consisted of aqueous 0.01 M trifluoroacetic acid (solvent A) and methanol (solvent B), and the gradient method used was 0% B for 10 min, 0–50% B for 10–20 min, 50–0% B for 20–23 min and 0% B for 23–25 min. Same HPLC system and conditions were used for purification and analytical analyses. Tissue/organ radioactivity was measured using an automated 2480 Wizard 2 gamma counter (Perkin Elmer) with a 3-inch NaI(Tl) detector. All animal experiments followed the principles of laboratory animal care and were approved by the Institutional Animal Care and Use Committee of Emory University.

2.2. Chemistry and radiosynthesis

2.2.1. Synthesis of $Al^{19}F$-NODA-butyric acid ($Al^{19}F$-1)—A solution of NODA-butyric acid, **1** (0.08 g, 0.242 mM) and $AlCl_3$ (0.038 g, 0.289 mM) in water was adjusted to pH 4.0 using 1 M sodium acetate buffer. Reaction mixture was heated on boiling water bath for 15 min. NaF (0.05 g, 1.21 mM) was added to the above reaction mixture and heated for another 30 min. Complex formation was confirmed by ESI-Mass analysis of reaction mixture. Product was purified by RP-HPLC (Water/MeOH; 0 to 70 % of MeOH for 30 min). Collected fraction was lyophilized after removing the organic solvent to obtain white fluffy solid *$Al^{19}F$*-**3** (0.044 g, 49%). ^1H NMR (D_2O, 400 MHz, 25 °C): δ 1.75 (q, 2H), 2.28–2.18 (m, 2H), 3.37–2.68 (m, 14H), 3.44 (s, 1H), 3.51–3.49 (d, 2H, J = 8 Hz), 3.55 (s, 1H). HRMS calcd for $C_{14}H_{24}AlFN_3O_6$, 376.14646; found, 376.14611 $[M + H]^+$.

2.2.2. ^{18}F Labeling—An aqueous ^{18}F solution [~ 1 mL, 1–1.85 GBq (27–50 mCi)] was loaded onto an anion exchange resin cartridge (that was prewashed with 1 mL of low ^{19}F water), washed with 2 mL of low ^{19}F water, and the ^{18}F isotope was then eluted from the cartridge with a 0.9% saline solution (0.4 mL) into a sealed 2 mL vial. Al^{18}F was prepared by adding a stock solution of $AlCl_3$ (22 μL of 2 mM in 0.1 M sodium acetate buffer pH 4 solution) to the ^{18}F saline solution and incubating the mixture at room temperature for 5 min. To the prepared Al^{18}F solution, the NODA-butyric acid ligand (**1**) (0.5 mL of 1 mg/mL in 0.1 M acetate buffer pH 4 solution) was added and the labeling mixture was heated at 110 °C for 15 min. The labeling mixture was purified by HPLC to remove the unchelated Al^{18}F and unlabeled ligand, and to produce the final Al^{18}F-NODA-butyric acid complex (Al^{18}F-**1**) with ~ 95% radiochemical purity as confirmed by HPLC analyses (retention time - 8 min). The fractions containing Al^{18}F-**1** were combined. The product was diluted in phosphate buffered saline (PBS, pH 7.4) to dilute any remaining organic solvent to less than 1% (v/v), and evaluated by HPLC for up to 4 h to assess complex in vitro stability. The PBS solution of Al^{18}F-**1** was used for in vivo studies. Total synthesis time was around 50–60 min including purification and formulation.

2.4. Biodistribution Studies

Al^{18}F-**1** was evaluated in two experimental groups of rats (Sprague–Dawley, 187–224 g each, Charles River, MA). Rats in both groups were anesthetized with ketamine–xylazine (2 mg/kg of body weight) injected intramuscularly, with additional supplemental anesthetic as needed. In the first group of 16 normal rats (Group A), the bladder was catheterized by use of heat-flared PE-50 tubing (Becton, Dickinson and Co.) for urine collection. The second group of 5 rats (Group B) was prepared to produce a model of renal failure. In that group, the abdomen was opened by a midline incision and both renal pedicles were identified and ligated just before radiotracer administration; thus, no urine was collected.

Each rat was injected intravenously via a tail vein with a 0.2 mL of a solution containing Al^{18}F-**1** (3.7 MBq/mL [100 μCi/mL]) and ^{131}I-OIH (925 kBq/mL [25 μCi/mL]) in PBS pH 7.4. One additional aliquot of the ^{18}F and ^{131}I tracer solution (0.2 mL) for each time point was diluted to 100 mL, and three 1-mL portions of the resulting solution were used as standards.

In Group A, eight animals were sacrificed at 10 min, and eight animals were sacrificed at 60 min after injection. A blood sample was obtained, and the kidneys, heart, lungs, spleen, stomach and intestines were removed and placed in counting vials. The whole liver was weighed, and random sections were obtained for counting. Samples of blood and urine were also placed in counting vials and weighed. Each sample and the standards were counted for radioactivity by using an automated gamma-counter; counts were corrected for background radiation and physical decay. The percentage of the dose in each tissue or organ was calculated by dividing the counts in each tissue or organ by the total injected counts. The percentage injected dose in whole blood was estimated by assuming a blood volume of 6.5% of total body weight. Four rats in Group A probably became hypotensive during the study since one rat in the 10-min group and 3 rats in the 60-min group produced almost no urine and those rats were eliminated from the combined data analysis. The Group B rats were sacrificed 60 min after injection and selected organs and blood were collected and analyzed as described above for Group A.

2.5. Metabolite studies

The solution of Al^{18}F-**1** [7.4 MBq (0.2 mCi)] was injected via tail vein into two additional rats prepared as in Group A. Urine was collected for 15 min and analyzed by HPLC to determine in vivo stablility of Al^{18}F-**1**.

2.6. PET/CT imaging

Small animal PET imaging was conducted according to the Emory Center for Systems Imaging (CSI) Standard Operating Procedure (SOP) and performed by CSI technical staff. Sprague-Dawley rats were initially anesthetized with ketamine/xylazine mixture injected intramuscularly and an acute intravenous catheter was placed in the rat's tail vain for administration of radioligand. Each imaging session included one rat placed on the scanner bed of the Inveon MicroPET/CT with a nose cone used to maintain anesthesia at 1–2% isofluorane at a flow rate of 500–1000 mL/min O_2. The rat was positioned in the tomograph on a resistive heating pad with rectal temperature probe feedback, and then fitted with a mini-clip for heart rate and blood oxygenation to allow physiological monitoring during the procedure. A dose of approximately 0.3–0.5 mCi/0.2mL of $Al^{18}F$-**1** was injected via tail vein at the start of the PET scan. Dynamic small-animal PET data were acquired over a period of 60 min after injection, followed by the acquisition of CT data over a period of 1 min. The CT was added for anatomical orientation. At the conclusion of the study, the rat was sacrificed prior to regaining consciousness. Images were reconstructed by OSEM3D/MAP using measured attenuation correction from a Co-57 point source. Image data were decay-corrected to the time of injection.

2.7. Statistical Analysis

All results are expressed as the mean ± SD. To determine statistical significance of differences between 2 groups at the same time point, comparisons were made using the 2-tailed Student *t* test for paired data; $P < 0.05$ will be considered to be statistically significant.

3. Results and Discussion

3.1. Chemistry

The synthesis of the labeling precursor **1** has been described previously [31]. Generally, NODA-butyric acid (**1**) was synthesized from 1,4,7-triazacyclononane via *N*-alkylation with *tert*-butyl bromoacetate to get a disubstituted intermediate by a pH-controlled workup method, followed by the reaction with *tert*-butyl bromobutyrate to yield the final ligand **1** as a hydrochloride salt.

The non-radioactive $Al^{19}F$-**1** was synthesized as a reference standard for characterizing the radioactive $Al^{18}F$-NODA-butyric acid complex ($Al^{18}F$-**1**) by HPLC. Complex $Al^{19}F$-**1** was obtained by reacting the ligand **1** with $AlCl_3$ in sodium acetate buffer (pH 4.0), followed by the addition of NaF and heating. Formation of complex $Al^{19}F$-**1** was confirmed by a molecular ion peak by mass/ion spray positive ionization (MS/ESI^+) analysis and the complex was purified by reverse phase high performance liquid chromatography (RP-HPLC). ^1H NMR analysis of the purified complex $Al^{19}F$-**1** supported the previously reported structural analysis of the similar compound [31]. The ^1H NMR spectrum of $Al^{19}F$-**1** showed the methylene protons of the acetate pendent arms as a pair of doublets at δ 3.57 and 3.46 ppm confirming the coordination of these two acetate moieties with aluminium fluoride during complex formation and the interaction of these protons with central fluoride atom. The $–NCH_2CH_2N–$ ring protons and $–NCH_2CH_2CH_2CO_2–$ alkyl chain protons produced overlapping multiplets centered at the region from δ 1.71 to 3.37 ppm, which shows asymmetrical methylene protons in the diastereotopic ring after complex formation as well as the unequivalent methylene protons of the dangling butyric acid arm. These multiplet patterns and chemical shifts of the chelate's protons in aqueous solution are similar and in the range usually found in analogous Al(III) complexes [27, 31, 32].

3.2. Radiochemistry

The radioactive $Al^{18}F$-**1** complex (Fig. 1) was obtained through a one-pot, two-step radiolabeling process by reacting the preformed $(Al^{18}F)^{2+}$ moiety with the NODA-butyric acid ligand **1** in aqueous solution [31]. Using this approach, the laborious but critical azeotropic drying step performed in the traditional radiofluorination procedure was eliminated. The ^{18}F radiotracer was isolated by HPLC with high radiochemical purity of > 95%, although it may be possible to develop a simpler purification step using solid phase extraction (SPE) cartridges as previously reported for other $Al^{18}F$ radiotracers [27, 29, 31]. The radiotracer was formed as a single species with well-established structure based on the analytic characterization of its ^{19}F analog and its identity was confirmed by using the cold compound $Al^{19}F$-**1** as a reference, since the radioactive and nonradioactive AlF complexes are chemically identical and have similar retention times. Since the radiolabeling reaction and the HPLC purification took place at low pH, the collected fraction containing $Al^{18}F$-**1** needed to be buffered at physiological pH before using the radiotracer for *in vivo* animal experiments. We expected that $Al^{18}F$-NODA-butyric acid complex would be monoanionic at pH 7.4 with the negative charge associated with the dangling $–(CH_2)_3CO_2^-$ group (Fig. 1). This charge distribution is shared by ^{131}I-OIH (Fig. 1) which shows a rapid plasma clearance, efficient tubular extraction and rapid rate of renal excretion. The simple, one-pot, aqueous ^{18}F radiolabeling method via $Al^{18}F$ chelation procedure yields $Al^{18}F$-**1** in high radiolabeling efficiency [31]; this method will facilitate kit development since there are no organic solvents to be removed prior to clinical use and it may be possible to eliminate the HPLC purification step using SPE. A lyophilized kit, requiring only the addition of saline solution of ^{18}F-fluoride, will not only facilitate fast and reproducible labeling procedure, but it also has the advantage of increasing the availability of ^{18}F radiotracers for *in vivo* experiments by eliminating the need for hot cells or a PET radiochemistry facility.

3.3. Stability

The $Al^{18}F$-NODA-butyric acid radiotracer showed high *in vitro* stability at physiological pH at room temperature. No measurable decomposition was observed when samples of incubated solution were analyzed by HPLC over 4 hours indicating that the tracer did not release $Al^{18}F$.

The urine of two rats collected for 15 min after the $Al^{18}F$-NODA-butyric acid injection was also analyzed by HPLC to determine the radiotracer's $Al^{18}F$-**1** *in vivo* stability and only the intact radiolabeled parent compound was observed, confirming that the tracer was excreted unchanged (Fig. 2), and that the all radioactivity was bound by $Al^{18}F$-**1**. Our findings are in agreement with earlier reports on the *in vitro* and *in vivo* stability of $Al^{18}F$ radiotracers [26, 27, 30, 33, 34].

3.4. Biodistribution

The pharmacokinetic properties of $Al^{18}F$-NODA-butyric acid were compared to those of ^{131}I-OIH, the clinical gold standard for the measurement of ERPF, in normal rats (Group A) and in a rat model with simulated complete renal failure (Group B). ^{18}F and ^{131}I tracers were simultaneously injected via the rat's tail vein and animals were sacrificed at 10 or 60 min post-injection in Group A and at 60 min post-injection in Group B. The biodistribution results, expressed as a percentage of injected dose (% ID) for selected organs/tissues, blood and urine are presented in Table 1.

In normal rats, the $Al^{18}F$-NODA-butyric acid tracer demonstrated high specificity for renal excretion; its urine activity, expressed as a percentage of ^{131}I-OIH, was 58 ± 4 % at 10 min and 92 ± 3 % at 60 min (Table 1). $Al^{18}F$-**1** was cleared rapidly from the blood but not as rapidly as ^{131}I-OIH; the %ID of $Al^{18}F$-**1** in blood at 10 min and 60 min was 8.5 ± 0.8 % and

1.6 ± 0.3 %, respectively, vs. 5.1 ± 0.5 % and 0.8 ± 0.1 %, respectively, for ^{131}I-OIH. However, there was minimal gastrointestinal activity recorded for the Al^{18}F tracer (1.2% at 10 min and 0.7% at 60 min) and that activity was lower at both time points than that measured for ^{131}I-OIH (P = 0.03 for 10 min and P = 0.0007 for 60 min). Total injected activity of Al^{18}F-**1** present in the heart, lung and spleen was negligible (less than 0.3%).

Al^{18}F-NODA-butyric acid is probably eliminated by both glomerular filtration and tubular secretion. Our previous studies of ^{125}I-iothamalate, a GFR marker, and ^{131}I-OIH in Sprague-Dawley rats have shown that the clearance of ^{125}I-iothamalate is 40% of the clearance of ^{131}I-OIH [35]. Consequently, if none of the Al^{18}F-**1** is protein bound and none of the Al^{18}F-**1** is secreted by the tubules, then the maximum Al^{18}F-**1** clearance would be 40% of the ^{131}I-OIH clearance. The excretion of Al^{18}F-**1** in the urine at 10 min provides an indirect measurement of plasma clearance. We demonstrated that the ratio of Al^{18}F-**1** to ^{131}I-OIH in the urine at 10 min was 58%, substantially greater than the 40% maximum from GFR alone. This result indicates that a component of Al^{18}F-**1** clearance must be due to secretion by the renal tubules. As anionic tracer, Al^{18}F-NODA-butyric acid likely shares the same tubular transport as ^{131}I-OIH and ^{99m}Tc-MAG3; however, this hypothesis will need to be confirmed by subsequent studies.

Al^{18}F-NODA-butyric acid was also compared to ^{131}I-OIH in rats with ligated renal pedicles to determine if complete renal failure would accelerate elimination via hepatobiliary excretion. As expected, renal failure slightly increased the liver and bowel activity of both tracers at 60 min but the new Al^{18}F radiotracer had significantly less liver and bowel activity than the ^{131}I-OIH gold standard (P < 0.001) (Table 1). ^{131}I-OIH had higher retention in the blood than Al^{18}F-**1** (P = 0.009) in the rats with renal pedicle ligation; this higher retention may be related to a higher plasma protein binding of ^{131}I-OIH compared to Al^{18}F-**1** resulting in lower volume of distribution for ^{131}I-OIH and a higher plasma concentration although this is speculative since plasma protein binding was not measured in this study. It is possible that a relatively low uptake of free ^{18}F or Al^{18}F-**1** in the bone may have resulted in a larger volume of distribution of Al^{18}F-**1** due to the relatively large bone mass and may explain the lower plasma concentration in the rats with ligated renal pedicles (see below PET/CT section). Future studies of second generation Al^{18}F-NODA derivatives should include measurements of plasma protein binding and bone activity to investigate this possibility. The percent injected dose remaining in the spleen, heart and lung for both ^{18}F and ^{131}I radiotracers were all less than 1%.

The potential of Al^{18}F-NODA-butyric acid as a renal tracer was previously suggested based on biodistribution studies in mice which revealed high uptake in the kidney at 10 min and substantial reduction at 60 min [31, 36]. Our studies extend this observation by direct comparison with the standard for evaluation of effective renal plasma flow, ^{131}I-OIH, showing that Al^{18}F-**1** has suitable pharmacokinetic properties as the renal PET agent. Results obtained from the simulated renal failure model are also important since they show that Al^{18}F-**1** retains its high specificity for renal excretion in renal failure and elimination from the body does not shift to hepatobiliary excretion. If a renal tracer is not highly specific for renal excretion in patients with impaired renal function, the clearance of that tracer will not provide an accurate measurement of renal function; moreover, activity in the liver, gallbladder and intestine can compromise scan interpretation [37].

3.5. PET/CT

Fused PET and CT scans are shown in Figs. 3 and 4. The preliminary small-animal dynamic PET performed on normal rats with the Al^{18}F-NODA-butyric acid tracer supported the biodistribution data and confirmed that the radiotracer was rapidly taken up by the kidneys

and excreted into bladder (Fig. 3). Additional images with the intensity adjusted to emphasize background activity and activity concentration in organs with low levels of uptake (Fig. 4) demonstrate minimal uptake in the spine which may be related to blood pool, marrow uptake, uptake in the bony matrix or a combination of the above. Both ^{18}F-fluoride and non-chelated Al^{18}F are known for high bone uptake [21, 22, 33].

4. Conclusions

Al^{18}F-NODA-butyric acid (Al^{18}F-**1**) was successfully prepared and its identity was confirmed by comparison with the fully characterized cold analog, Al^{19}F-NODA-butyric acid (Al^{19}F-**1**). The radiolabeled complex Al^{18}F-**1** was isolated by HPLC with high radiochemical purity and was proven to be stable at physiological conditions for the duration of the animal experiments. Metabolite studies confirm that the tracer was excreted intact into the urine. Although the renal excretion of Al^{18}F-**1** is less than that of ^{131}I-OIH at 10 minutes in normal rats, the urine activity of these two tracers is nearly equal at 60 min. Biodistribution studies also show that Al^{18}F-**1** is cleared rapidly from the blood but more slowly than is ^{131}I-OIH. However, there is minimal gastrointestinal activity from the Al^{18}F-**1** tracer; lower at both 10 and 60 minutes time points than that from ^{131}I-OIH. Studies in rats with ligated renal pedicles showed higher liver and intestinal activities for both ^{18}F and ^{131}I tracers, but those increases are lower for Al^{18}F-**1** suggesting that renal failure results in less hepatobiliary excretion or intestinal secretion of the Al^{18}F tracer compared to ^{131}I-OIH. The results from microPET/CT imaging studies confirm the biodistribution results. In summary, we have demonstrated that Al^{18}F-NODA-butyric acid provides a facile labeling approach to the development of a PET renal tracer that has acceptable pharmacokinetic and chemical properties as a renal imaging agent. Further investigation of Al^{18}F-based compounds as PET radiotracers may offer a superior PET tracer that combines high quality images with a reliable measurement of effective renal plasma flow.

Acknowledgments

This work was funded by the National Institute of Health (NIH/NIDDK) grant R37 DK038842 (PI: Taylor) and partially by P50 CA128301-0002 (PI: Shim). MicroPET imaging was supported by the Emory Center for Systems Imaging (CSI) pilot grant (PI: Lipowska). The authors thank Eugene Malveaux for his excellent technical assistance with all animal experiments and the Emory CSI Radiopharmacy for ^{18}F-fluoride solution.

References

1. Prigent A. Monitoring renal function and limitations of renal function tests. Semin Nucl Med. 2008; 38:32–46. [PubMed: 18096462]
2. Lane BR, Poggio ED, Herts BR, Novick AC, Campbell SC. Renal function assesment in the era of chronic kidney disease: renewed emphasis on renal function centered patient care. J Urol. 2009; 182:435–44. [PubMed: 19524967]
3. Gates HF. Split renal function testing using Tc-99m DTPA: a rapid technique for determining differential glomerular filtration. Clin Nucl Med. 1983; 8:400–7. [PubMed: 6357589]
4. Shore RM, Koff SA, Mentser M, Hayes JR, Smith SP, Smith JP, et al. Glomerular filtration rate in children: determination from the Tc-99m-DTPA renogram. Radiology. 1984; 151:627–33. [PubMed: 6371888]
5. Fritzberg AR, Kasina S, Eshima D, Johson DL. Synthesis and biological evaluation of technetium-99m MAG3 as a hippuran replacement. J Nucl Med. 1986; 27:111–6. [PubMed: 2934521]
6. Taylor A, Eshima D, Fritzberg AR, Christian PE, Kasina S. Comparison of iodine-131 OIH and technetium-99m MAG3 renal imaging in volunteers. J Nucl Med. 1986; 27:795–803. [PubMed: 2940350]

7. Esteves FP, Taylor A, Manatunga A, Folks RD, Krishnan M, Garcia EV. ^{99m}Tc-MAG3 renography: normal values for MAG3 clearance and curve parameters, excretory parameters and residual urine volume. AJR. 2006; 187:W610–W7. [PubMed: 17114514]
8. Shanon A, Feldman W, McDonald P, Martin DJ, Matzinger MA, Shillinger JF, et al. Evaluation of renal scars by technetium-labelled dimercaptosuccinic acid scan, intravenous urography and ultrasonography: a comparative study. J Pediatr. 1992; 120:399–403. [PubMed: 1311376]
9. Pipesz A, Blaufox MD, Gordon I, Granerus G, Majd M, O'Reilly P, et al. Consensus on renal cortical scintigraphy in children with urinary tract infection. Scientific Committee of Radionuclides in Nephrourology. Semin Nucl Med. 1999; 29:160–74. [PubMed: 10321827]
10. Lipowska M, Marzilli LG, Taylor AT. ^{99m}Tc(CO)$_3$-nitrilotriacetic acid: a new renal radiopharmaceutical showing pharmacokinetic properties in rats comparable to those of ^{131}I-OIH. J Nucl Med. 2009; 50:454–60. [PubMed: 19223406]
11. Taylor AT, Lipowska M, Marzilli LG. ^{99m}Tc(CO)$_3$(NTA): a ^{99m}Tc renal tracer with pharmacokinetic properties comparable to those of ^{131}I-OIH in healthy volunteers. J Nucl Med. 2010; 51:391–6. [PubMed: 20150248]
12. Taylor AT, Lipowska M, Cai H. ^{99m}Tc(CO)$_3$(NTA) and ^{131}I-OIH: comparable plasma clearances in patients with chronic kidney disease. J Nucl Med. 2013; 54:578–84. [PubMed: 23424193]
13. Eshima D, Fritzberg AR, Taylor A. Tc-99m renal tubular function agents: current status. Semin Nucl Med. 1990; 20:28–40. [PubMed: 2136959]
14. Marcus CS, Kuperus JH. Pediatric renal iodine-123 orthoiodohippurate dosimetry. J Nucl Med. 1985; 26:1211–4. [PubMed: 3900309]
15. Lewis DM. ^{99}Mo supply - the times they are a-changing. Eur J Nucl Med. 2009; 36:1371–4.
16. Szabo Z, Xia J, Mathews WB, Brown PR. Future direction of renal positron emission tomography. Semin Nucl Med. 2006; 36:36–50. [PubMed: 16356795]
17. Szabo Z, Xia J, Mathews WB. Radiopharmaceuticals for renal positron emission tomography imaging. Semin Nucl Med. 2008; 38:20–31. [PubMed: 18096461]
18. Schnöckel U, Reuter S, Stegger L, Schlatter E, Schäfers KP, Hermann S, et al. Dynamic ^{18}F-fluoride small animal PET to noninvasively assess renal function in rats. Eur J Nucl Med. 2008; 35:2267–74.
19. Awasthi V, Pathuri G, Agashe HB, Gali H. Synthesis and in vivo evaluation of *p*-^{18}F-fluorohippurate as a new radiopharmaceutical for assessment of renal function by PET. J Nucl Med. 2011; 52:147–53. [PubMed: 21149490]
20. Pathuri G, Hedrick AF, Awasthi V, Gali H. Single-step radiosynthesis and in vivo evaluation of novel fluorine-18 labeled hippurate for use as a PET renal agent. Nucl Med Biol. 2012; 39:1195–201. [PubMed: 22898317]
21. Schirrmeister H, Guhlmann A, Elsner K, Kotzerke J, Glatting G, Rentschler M, et al. Sensitivity in detecting osseous lesions depends on anatomic localization: planar bone scintigraphy versus ^{18}F PET. J Nucl Med. 1999; 40:1623–9. [PubMed: 10520701]
22. Even-Sapir E, Metser U, Flusser G, Zuriel L, Kollender Y, Lerman H, et al. Assessment of malignant skeletal disease: initial experience with ^{18}F-fluoride PET/CT and comparison between ^{18}F-fluoride PET and ^{18}F-fluoride PET/CT. J Nucl Med. 2004; 45:272–8. [PubMed: 14960647]
23. Pathuri G, Sahoo K, Awasthi V, Gali H. Renogram comparison of *p*-[^{18}F]fluorohippurate with *o*-[^{125}I]iodohippurate and [^{99m}Tc]MAG3 in normal rats. Nucl Med Commun. 2011; 32:908–12. [PubMed: 21876402]
24. Smith GE, Sladen HL, Biagini SCG, Blower PJ. Inorganic approaches for radiolabelling biomolecules with fluorine-18 for imaging with Positron Emission Tomography. Dalton Trans. 2011; 40:6196–205. [PubMed: 21499604]
25. McBride WJ, Sharkey RM, Karacay H, D'Souza CA, Rossi EA, Laverman P, et al. A Novel Method of ^{18}F Radiolabeling for PET. J Nucl Med. 2009; 50:991–8. [PubMed: 19443594]
26. McBride WJ, D'Souza CA, Sharkey RM, Karacay H, Rossi EA, Chang CH, et al. Improved ^{18}F labeling of peptides with a fluoride-aluminum-chelate complex. Bioconjugate Chem. 2010; 21:1331–40.
27. D'Souza CA, McBride WJ, Sharkey RM, Todaro LJ, Goldenberg DM. High-yielding aqueous ^{18}F-labeling of peptides via Al^{18}F chelation. Bioconjugate Chem. 2011; 22:1793–803.

28. McBride WJ, Sharkey RM, Goldenberg DM. Radiofluorination using aluminum-fluoride ($Al^{18}F$). EJNMMI Research [Online]. 2013; 3:36.10.1186/2191-219X-3-36
29. McBride WJ, D'Souza CA, Karacay H, Sharkey RM, Goldenberg DM. New Lyophilized Kit for Rapid Radiofluorination of Peptides. Bioconjugate Chem. 2012; 23:538–47.
30. Wan W, Guo N, Pan D, Yu C, Weng Y, Luo S, et al. First experience of ^{18}F-Alfatide in lung cancer patients using a new lyophilized kit for rapid radiofluorination. J Nucl Med. 2013; 54:691–8. [PubMed: 23554506]
31. Shetty D, Choi SY, Jeong JM, Lee JY, Hoigebazar L, Lee YS, et al. Stable aluminium fluoride chelates with triazacyclononane derivatives proved by X-ray crystallography and ^{18}F-labeling study. Chem Commun. 2011; 47:9732–4.
32. de Sá A, Prata MIM, Geraldes CFGC, André JP. Triaza-based amphiphilic chelators: Synthetic route, in vitro characterization and in vivo studies of their Ga(III) and Al(III) chaelates. J Inorg Chem. 2010; 104:1051–62.
33. Laverman P, McBride WJ, Sharkey RM, Eek A, Joosten L, Oyen WJG, et al. A novel facile method of labeling octreotide with ^{18}F-Fluorine. J Nucl Med. 2010; 51:454–61. [PubMed: 20150268]
34. Shetty D, Jeong JM, Kim YJ, Lee JY, Hoigebazar L, Lee YS, et al. Development of a bifunctional chelating agent containing isothiocyanate residue for one step F-18 labeling of peptides and application for RGD labeling. Bioorg Med Chem. 2012; 20:5941–7. [PubMed: 22917858]
35. Taylor A Jr, Eshima D. Effects of altered physiologic states on clearance and biodistribution of technetium-99m MAG3, iodine-131 OIH, and iodine-125 iothalamate. J Nucl Med. 1988; 29:669–75. [PubMed: 2967354]
36. Shetty D, Jeong JM, Hoigebazar L, Lee Y, Lee D, Chung J, et al. Development of Al-F-18-NO2A-butyric acid complex as renal imaging radiopharmaceutical. J Nucl Med. 2011; 52 (Suppl. 2): 170P.
37. Rosen JM. Gallblader uptake simulating hydronephrosis of Tc-99m-MAG3 scintigraphy. Clin Nucl Med. 1993; 18:713–4. [PubMed: 8403709]

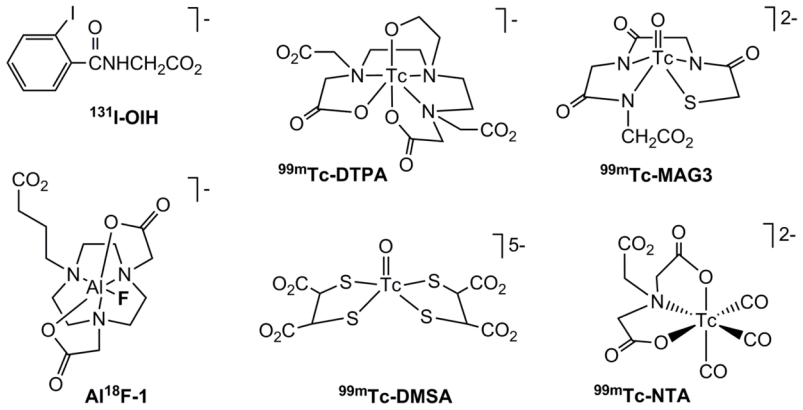

Figure 1.

The chemical structures of known ^{99m}Tc renal radiotracers and the new ^{18}F tracer evaluated in this study (AlF-**1**); tracers' overall charges of at physiological pH are included.

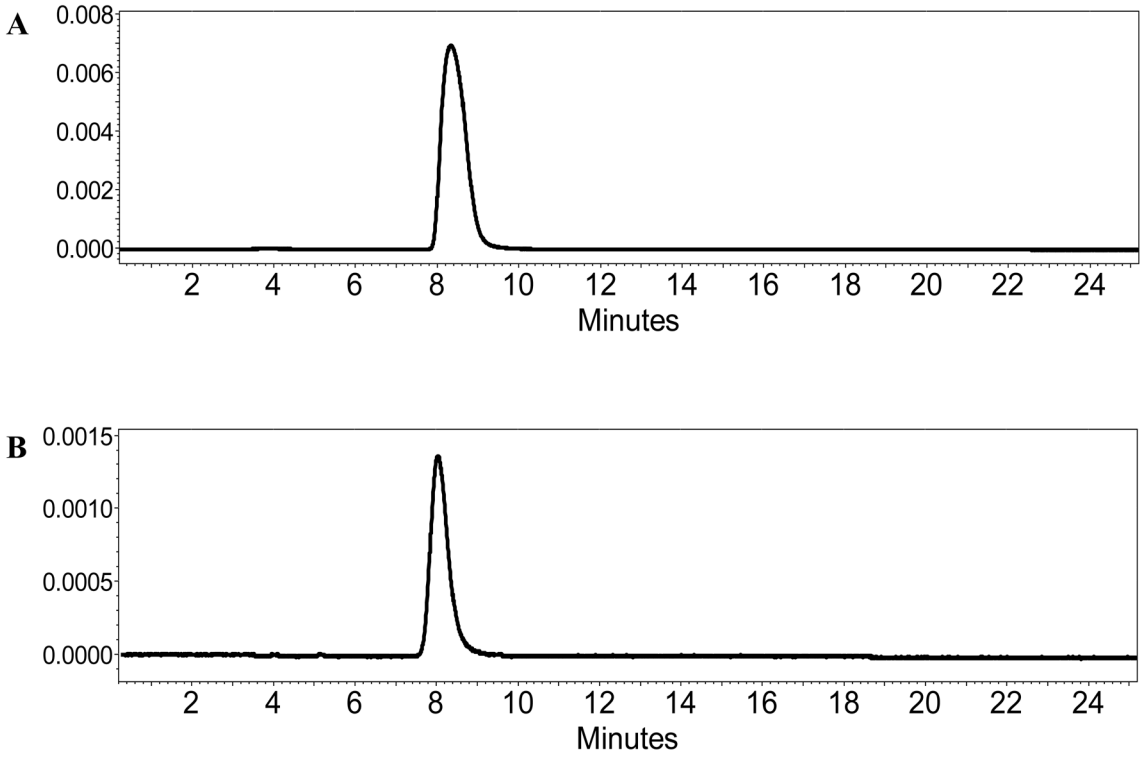

Figure 2.
HPLC of $Al^{18}F$-NODA-butyric acid before injection (A) and in the rat's urine at 15 min after injection (B).

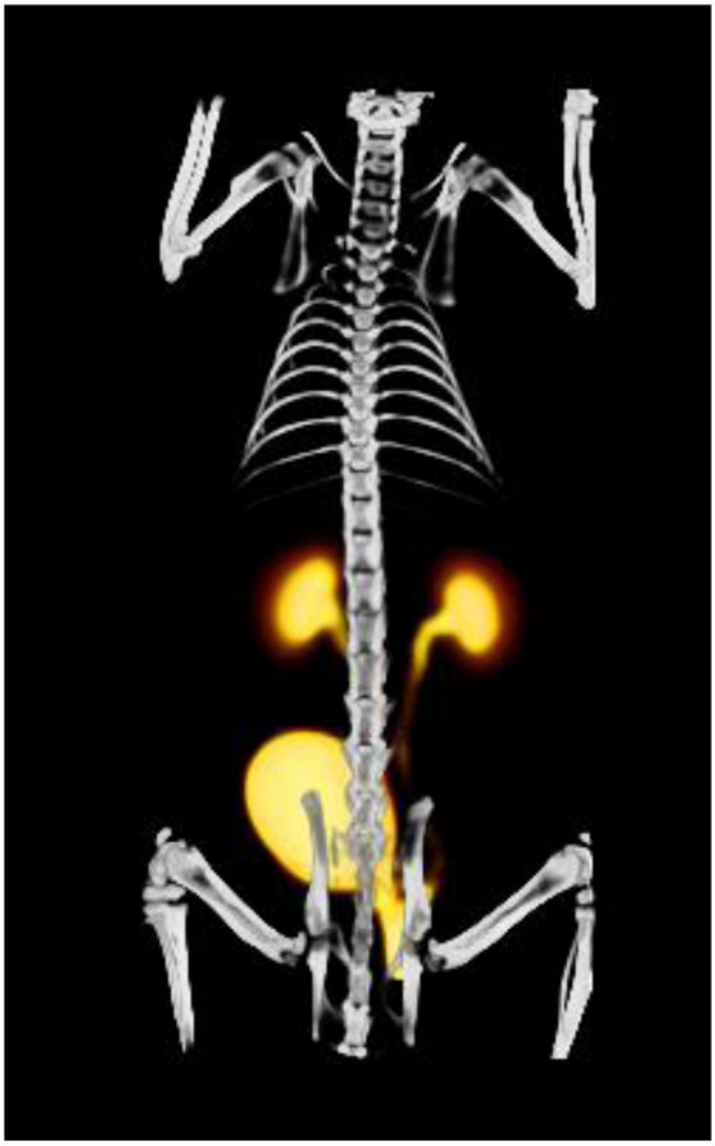

Figure 3.
Fused volume rendering of PET and CT of a normal rat injected with Al^{18}F-NODA-butyric acid. The PET image represents data summed from 5–60 min post-injection.

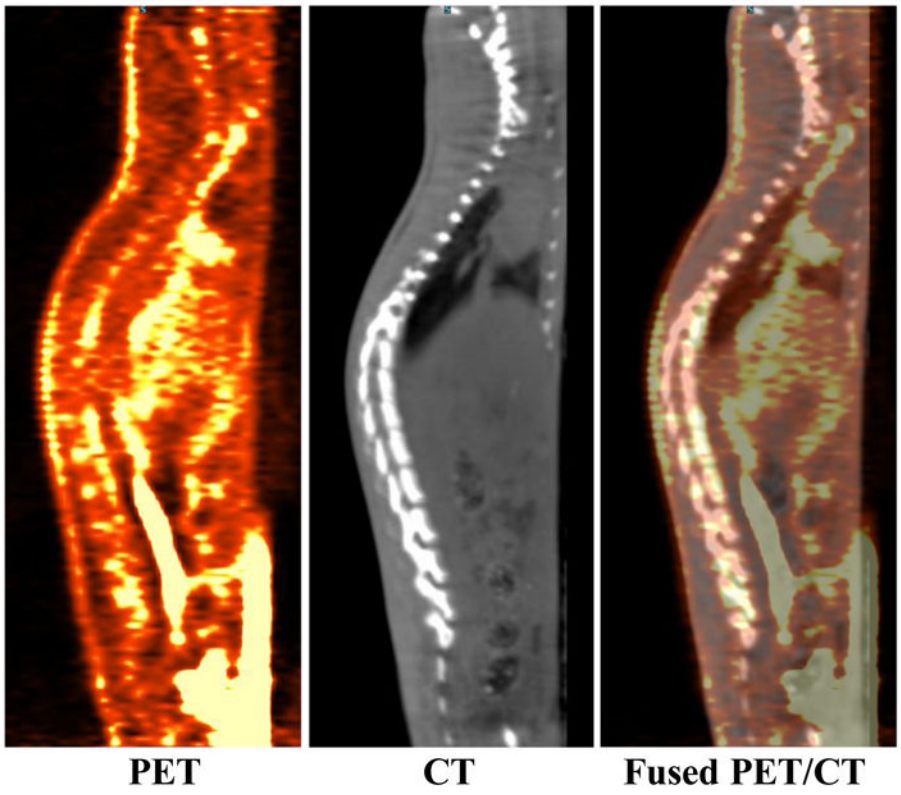

Figure 4.
PET (left), CT (middle) and fused PET/CT (right) sagittal images of Al^{18}F-NODA-butyric acid with intensity scaled to allow imaging of organs with low levels of activity. The PET image, obtained by summing data from 5–60 min post-injection, demonstrates activity in the spine however this may consists of blood pool activity, marrow activity, activity in the bony matrix or a combination of the above.

Table 1

Percent injected dose of Al^{18}F-NODA-butyric acid and ^{131}I-OIH in blood, urine and selected organs at 10 and 60 minutes in normal rats[a] (Group A) and in rats[a] with renal pedicle ligatation (Group B).

	Blood		Kidney		Urine			Liver		Bowel[b]	
	^{18}F	^{131}I-OIH	^{18}F	^{131}I-OIH	^{18}F	^{131}I-OIH	% ^{18}F / ^{131}I-OIH	^{18}F	^{131}I-OIH	^{18}F	^{131}I-OIH
Group A											
10 min	8.5 ± 0.8[c]	5.1 ± 0.5	4.6 ± 0.8[d]	5.3 ± 1.2	29.3 ± 3.7[c]	50.8 ± 5.2	58 ± 4	2.3 ± 0.4[c]	3.3 ± 0.2	1.2 ± 0.3[d]	1.7 ± 0.5
60 min	1.6 ± 0.3[c]	0.8 ± 0.1	1.9 ± 0.4[c]	0.7 ± 0.4	78.6 ± 4.8[c]	85.4 ± 3.1	92 ± 3	0.7 ± 0.1[e]	0.6 ± 0.2	0.7 ± 0.1[c]	1.8 ± 0.3
Group B											
60 min	13.5 ± 0.7[c]	15.1 ± 0.9	0.4 ± 0.1[e]	0.5 ± 0.2	-	-	-	4.0 ± 0.2[c]	7.1 ± 0.6	3.2 ± 0.6[c]	7.6 ± 1.1

Data are presented as mean ± SD.

[a](10 min n=7, 60 min n=5, lig.ped. 60 min n=5).

[b]Bowel includes intestines and stomach.

[c]$P < 0.001$,

[d]$P < 0.05$ and

[e]$P > 0.07$, comparison of biodistribution between Al^{18}F-NODA-butyric acid and ^{131}I-OIH.